J. Chem. Lett. 3 (2022) 135-143

Research Article

Journal of Chemistry Letters
journal homepage: www.jchemlett.com
ISSN (online) 2717-1892

Adsorption of SO_2 and NO_2 on ZrO_2 (1 1 0) Surface: Density Functional Theory and Molecular Dynamic Simulation Studies

Umaru Umar, Abdullahi Muhammad Ayuba*

Department of Pure and Industrial Chemistry, Faculty of Physical Sciences, Bayero University, Kano, Nigeria

ARTICLE INFO

Article history:
Received 2 July 2022
Received in revised form 3 August 2022
Accepted 11 September 2022
Available online 18 September 2022

Keywords:
Greenhouse gases
Zirconia surface
Molecular dynamic simulation
Density functional theory
Physical adsorption

ABSTRACT

In order to save the environment, there is an urgent need for control measures due to the rapidly rising concentration of greenhouse gases in the atmosphere. Density functional theory (DFT) and molecular dynamic simulation investigations were used in this study to examine the adsorption characteristics of SO_2 and NO_2 on zirconia surface. Several global reactivity parameters where analyzed as part of the DFT calculations. Compared to NO_2 (ΔE = 6.424eV), the zirconia surface is substantially more sensitive to SO_2 (ΔE = 5.415eV) capture, according to the observed DFT data. The findings of the quenched molecular dynamic simulations also showed that SO_2 (E_{ads} = -66.23kcal/mol) is more likely to adsorb on zirconia surface than NO_2 (E_{ads} = -57.50kcal/mol), despite the fact that both molecules obey the physical adsorption mechanism. SO_2 and NO_2 respectively bond to the ZrO_2 (1 1 0) surface due to the two molecules' favorable orientation, which is parallel to the surface with angles pointing upward. Zirconium oxide can find use as an effective adsorbent for the removal of SO_2 and NO_2 gases from air environments because of these discoveries.

1. Introduction

The presence of SO_2 and NO_2 in the atmosphere has a significant impact on air pollution, including acid rain, photochemical smog, greenhouse effect, and ozone layer depletion [1]. When sulfur-containing fossil fuels are burned in factories, car engines, power plants, and homes, SO_2 gas is released into the atmosphere. Acid rain is created when the subsequent SO_2 gas mixes with atmospheric moisture [2]. However, high-temperature combustion processes, electrical discharge during thunderstorms, and microbiological activities in the soil all produce NO_2 gas [3]. The main antecedent of photochemical smog is the resultant NO_2 gas in the atmosphere [4].

To maintain a friendly environment, it becomes a global task to reduce the amount of greenhouse gases in the atmosphere [5]. Researchers spent a significant amount of effort and resources in developing effective methods to remove these dangerous gases from the environment [6]. Due to its low operating cost, effectiveness, simplicity of construction, and sensitivity towards gases, sensing gas molecules to capture the pollutant gases by adsorption is considered to be a method of choice. This is among the various methods developed to counteract the effect of greenhouse gases in the atmosphere [7]. Metal oxides have reportedly attracted a lot of attention among the various materials used to trap polluting gases from the atmosphere because of their wide range of applications [8].

Zirconia is a crystalline zirconium dioxide with mechanical characteristics resembling those of the metals to which it is analogous [9]. There are three different types of zirconia: mono-clinic, cubic, and tetragonal [10]. Numerous scientists have used experimental approaches, such as infrared spectroscopy and micro calorimetry techniques, to investigate the adsorption characteristics of gaseous contaminants on zirconia surfaces [11–13]. In hydrous zirconia gels, the origin of porosity was examined by Gimblett et al. [14].

* Corresponding author. Tel.: +2348062771500; e-mail: ayubaabdullahi@buk.edu.ng

To the best of our knowledge, no known research has tested the effectiveness of SO_2 and NO_2 molecules adsorbing on zirconia surface using a computational technique. In order to examine the sensitivity and mechanism of zirconia surface toward the adsorptive capture of SO_2 and NO_2 polluting gases from the environment, the current research used a theoretical approach.

2. Results and Discussion

2.1 Frontier molecular orbital distribution

It is demonstrated that the electronic distribution of the Frontier molecular orbitals (HOMO and LUMO) of the reacting species completely determines the reactivity of molecules [15]. As a result, it is crucial to analyze the orbital distribution of the molecules under study to obtain accurate information about their molecular reactivity. The ability of molecules to donate electrons is associated with HOMO, whereas the ability to accept electrons is associated with LUMO [16]. The structures of optimized molecules, as well as their HOMO and LUMO distribution, are shown in Figure 1. From Figure 1, the HOMO and LUMO can be observed to be evenly distributed throughout the SO_2 molecule, indicating that both the sulphur and oxygen atoms in the molecule have the ability to donate electrons to ZrO_2 (1 1 0) as well as accept electrons from the ZrO_2 (1 1 0) through back bonding to establish feedback bonds. Unlike the LUMO distribution, which is not concentrated on the nitrogen atom in NO_2, this suggests that it is unable to participate in taking electrons from ZrO_2 (1 1 0). The HOMO orbital distribution for NO_2 is identical to that of SO_2. This may be explained by the fact that the presence of extra electronegative atoms (oxygen) flanked on both sides of nitrogen in NO_2 and sulphur in SO_2 has significantly inhibited its propensity to take electrons.

2.2 *Orbital energies and their derived parameters*

It is thought that the analysis of the Frontier molecular orbital energies and the derived parameters including E_H, E_L, ΔE, ω, χ, η, ε, ΔN_{max}, $\Delta E_{b\text{-}d}$ etc, are important DFT parameters that can forecast a molecule's reactivity with respect to an adsorbent surface and the relationship between that reactivity and structure [17]. Table 1 displays the quantum chemical parameters determined from the Frontier molecular orbital energies by calculation. While E_L refers to a molecule's ability to accept electrons, E_H often refers to a molecule's ability to donate electrons [18]. One key factor that affects molecular reactivity is the energy gap (ΔE) between the HOMO and LUMO [19]. Because transferring an electron from the last occupied molecular orbital to the next accessible orbital requires energy, the higher the ΔE value, the less molecular reactivity. Therefore molecular reactivity increases with decreasing ΔE value [20]. Table 1 shows that when compared to NO_2 (6.424eV), SO_2 has a substantially lower ΔE value (5.415eV). It can therefore be inferred from the ΔE value that SO_2 is expected to be more firmly adsorbed on ZrO_2 (1 1 0) surface than NO_2. The hard-soft-acid-base (HSAB) principle, which holds that hard acids prefer to attach to hard bases whereas soft acids prefer to bond to soft bases [22], explains the nature of molecular interaction on adsorbent surfaces [39]. Since the zirconia surface is a soft acid in this situation, a softer base is necessary for an effective binding strength. In this regard, it can be concluded from Table 1 that SO_2 with a softness value of 0.369 eV^1 is greater than and will interact with zirconia surfaces more strongly and effectively than NO_2 with a softness value of 0.311 eV^{-1}.

According to equation 8, the number of electrons transported (ΔN_{max}) was computed. The results are shown in Table 1. As can be observed, the values are both positive (1.097 eV for SO_2 and 0.786 eV for NO_2), indicating that the exchange of electrons between the gases and the zirconia surface is favorable. According to Verma et al. [23], the adsorption strength increases as the gases' ability to donate electrons increases. The superiority of SO_2 binding susceptibility on zirconia surface over NO_2 is further confirmed by this parameter. Additionally, the energy of back donation ($\Delta E_{b\text{-}d}$) principle was used to assess the interaction between the molecules of the examined gases (NO_2 and SO_2) and the zirconia surface. $\Delta E_{b\text{-}d}$ is the energy change that occurs when a molecule gets energy and then donates it back [24]. According to Gomez et al. [25] and Obi-Egbedi et al. [26], the stabilization energy concept can be used to explain the reason for stronger adsorption energy between the adsorbate molecule and the adsorbent surface. The lesser the negative value is, the better the process of back donation. In light of this, we can say that zirconia is more effective in absorbing SO_2 (-0.677eV) than NO_2 (-0.803eV). The inverse of electrophilicity ($1/\omega$) called nucleophilicity (ε) denotes the propensity of molecules to donate or share electrons, whereas the electrophilicity index (ω) denotes the capacity of molecules to accept electrons [27]. According to literature, compounds with high nucleophilicity values are more adsorptive, whereas those with high electrophilicity index values are less adsorptive [28]. It is clear from Table 1 that SO_2 molecule has the lowest electrophilicity index and the highest nucleophilicity, making it relatively a better adsorbate on the ZrO_2 surface than the NO_2 molecule.

Table 1. Quantum chemical parameters of the studied molecules

Molecule	**SO_2**	**NO_2**
E_H (eV)	-8.646	-8.263
E_L (eV)	-3.231	-1.839
ΔE (eV)	5.415	6.424

η (eV)	2.708	3.212
σ $(eV)^{-1}$	0.369	0.311
χ (eV)	5.939	5.051
ω (eV)	6.512	3.972
ε $(eV)^{-1}$	0.154	0.252
ΔN_{max}	1.097	0.786
ΔE_{b-d} (eV)	-0.677	-0.803

2.3 Local and Global Reactivity

Molecules are known to interact with metal surfaces by donating, accepting or exchanging electron(s). Understanding the mechanism of electron transfer is crucial, since doing so can reveal the active site(s) on the molecules under study. The Fukui indices were used as local reactivity indicators to access the active regions of interaction within the molecules under nucleophilic (f^+), electrophilic (f^-), and radical (f^o) attack conditions. The nucleophilic, electrophilic and radical points of attack are controlled by the maximal threshold values of f^+, f^-, and f^o. The targets of nucleophilic attacks are the atoms with the highest value of f^+. Similar to this, when f^- has the maximum value, electrophilic attacks are preferred. Condensed Fukui functions of the investigated molecules are listed in Table 2. The Table shows that for the f^-, f^+, and f^o indices, NO_2 has the largest Mulliken and Hirshfeld charges on O(1), O(1), and O(3) atoms. This suggests that the two flanking oxygen atoms in NO_2 molecule are vulnerable to electrophilic and nucleophilic attack. For SO_2, the sulphur atom of the molecule yielded the greatest Mulliken and Hirshfeld values for the f^-, f^+, and f^o indices. This shows that the SO_2 molecule's center of reactivity for electrophilic, nucleophilic, or radical atoms is located on the sulphur atom.

Table 3 displays the calculated proportion of the second-order Fukui function for the investigated molecules, while Figure 2 displays their graphical representations. Values from Table 3 show that for both the Mulliken and Hirshfeld charges for SO_2 and NO_2, 33.33% of the items in Figure 4 had positive values of the Fukui second order function ($f^2 > 0$), while 66.67% had negative values ($f^2 < 0$). The two molecules' second order Fukui functions indicate that they are both nucleophilic in terms of their overall reactivity.

2.4 Molecular Dynamic (MD) simulation

The Forcite module in the Acceryls Materials Studio 7.0 program was used to conduct the MD simulation of the interaction between the adsorbate gases and the zirconia surface in order to study their adsorption behavior. The MD simulation was run for 5000 steps to quench at every 250 steps in order to reduce the system's temperature and energy. Figure 3 shows the equilibrium configuration of the gases on the ZrO_2 (1 1 0) surface. The figure clearly shows that the two gases were properly oriented for adsorption on the zirconia surface and that both S and O atoms (for SO_2) and N and O atoms (for NO_2) were structurally adjusted.

Equation 13 was used to calculate the adsorption energy of the interaction, while equation 14 was utilized to determine the binding energy of each gas molecule to the ZrO_2 (1 1 0) surface. This was done to be able to tell how strong of a bond or interaction there was between the two gases on the ZrO_2 (1 1 0) surface [20]. It is clear from Table 4 that both compounds' adsorption energies are significantly negative, which points to a successful adsorption process [29]. Additionally, the Table shows that the adsorption energy of SO_2 (-66.23 $kcalmol^{-1}$) is considerably larger than that of NO_2 (-57.50 $kcalmol^{-1}$), indicating that ZrO_2 (1 1 0) is likely to have a stronger affinity for SO_2 from the environment than NO_2 because SO_2 is more sensitive to its surface than NO_2. All of the gaseous molecule interactions with the ZrO_2 surface had adsorption/binding energies that were less than $\pm$100 $kcalmol^{-1}$, which is the cutoff point that distinguishes between physical and chemical adsorption mechanisms [30]. A strong physisorption mechanism can be inferred to explain the process based on the values of the adsorption/binding energies of the gases on the metal surfaces.

The ***measure/distance*** module in Acceryls Material Studio 7.0 was used to determine the distances between the adsorbate molecules and ZrO_2 (1 1 0) surface and the results were listed in Table 4. Shorter bond distances between linked atoms indicate stronger interactions, therefore we conclude that SO_2 is more favorably adsorbed on ZrO_2 (1 1 0) than NO_2 based on the distances, which are more than 3.5Å with SO_2 (d = 3.51Å) closer to the surface than NO_2 (d = 3.55Å). It is further hypothesized that there may be physical interaction between the molecules and the zirconia surface at bond lengths larger than 3.5Å, as described by Belghitti et al. [31].

Additionally, the atomic radii of the two bonded atoms are much higher than the shortest adsorption bond distances (d) between the nearest atoms of the molecules to the zirconia surface (S-ZrO_2 for SO_2 and N-ZrO_2 for NO_2). According to Pyykko and Atsumi [32], ZrO_2 and S have an atomic radius sum of 2.57Å, while ZrO_2 and N have an atomic radius total of 2.25Å. When these are compared to the shortest adsorption bond distances between the molecules and the zirconia surface listed in Table 4, these values are relatively distances shorter. According to Ye et al. [33], if the difference is greater than $\pm$0.3Å, the interaction between the two linked atoms does not entail a chemical bond, hence it is safe to assume that the two gases were physically adsorbed onto the zirconia surface

The hollow (H), bridge (B), and top (T) of the zirconia surface are the three distinct adsorption sites for housing the gas molecules, respectively (Figure 4a) [34]. Kulishi et al. [35] suggested that the hollow was the most reliable adsorption location. Additionally, the two molecules interact with the zirconia surface in three different configurations: the two parallel to the surface (O-S-O and O-N-O angles facing downward) bind oxygen to the surface (Figure 4b); the two perpendicular to the surface bind oxygen to the surface (Figure 4c); and the two parallel to the surface (O-S-O and O-N-O angles facing upward) bind S for SO_2 and N for NO_2 to the surface, respectively (Figure 4d). The final configuration out of the three provides the highest adsorption energy; as a result, it was chosen for adsorption on the hollow site in all simulations.

The molecules' bond lengths and bond angles before and after adsorption where compared and the results are as shown in Table 5. It is evident that both molecules underwent some significant geometrical modifications during adsorption. S-O and N-O bonds have been lengthened by 0.37 and 0.30Å, respectively. Similar to bond lengths, the O-N-O bond angle increased by 3.160°, while the O-S-O bond angle decreased by 9.260°. After adsorption, the molecules' bonds and bond angles underwent a significant shift, indicating that there was significant contact between the molecules and the zirconia surface [29].

2.5 Electronic and geometric structure

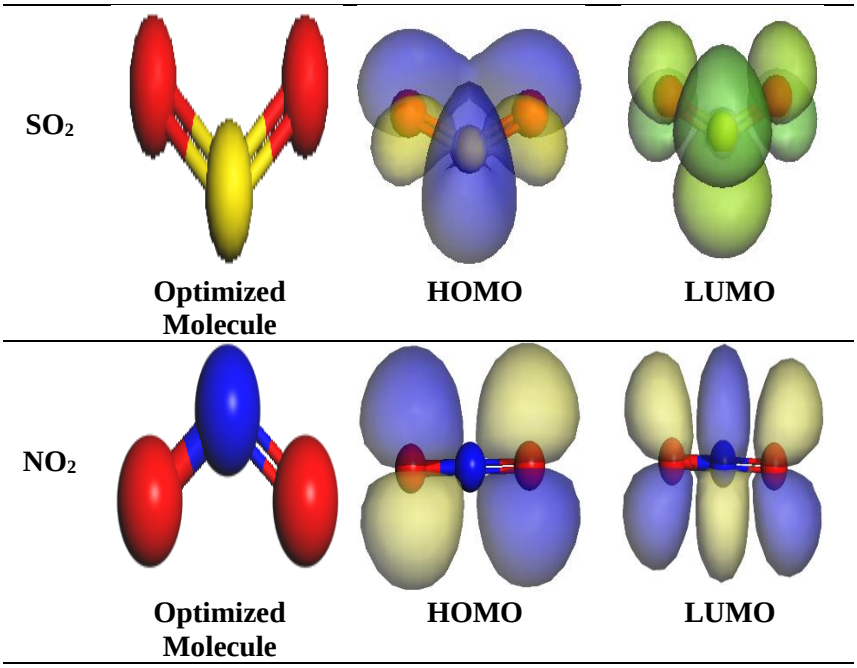

Figure 1. Electronic and structural properties of optimized SO_2 and NO_2

Table 2. Calculated Fukui Functions of the studied Molecules

	f^-		f^+		f^o	
Atom	Mulliken	Hirshfeld	Mulliken	Hirshfeld	Mulliken	Hirshfeld
			NO_2 Molecule			
O_1	0.414	0.404	0.351	0.352	0.382	0.378
N_2	0.178	0.192	0.301	0.296	0.239	0.244
O_3	0.408	0.404	0.348	0.352	0.378	0.378
			SO_2 Molecule			
S_1	0.395	0.423	0.420	0.429	0.407	0.426
O_2	0.303	0.289	0.290	0.286	0.296	0.287
O_3	0.303	0.289	0.290	0.286	0.296	0.287

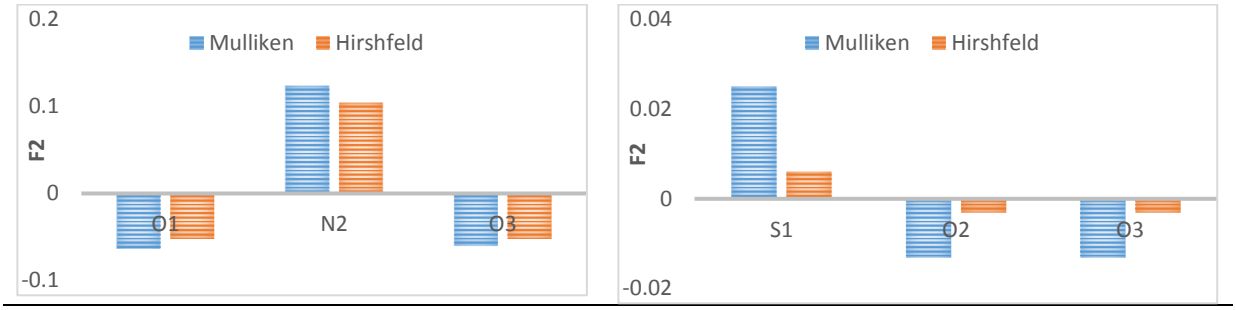

NO_2 **SO_2**

Figure 2. Second-order Fukui function of the studied compounds

Table 3. Calculated percentage of second- order Fukui function of the studied inhibitor molecules

Molecules	**Nucleophilic (F^{2+})**		**Electrophilic (F^{2-})**	
	Mulliken	Hirshfeld	Mulliken	Hirshfeld
NO_2	33.33	33.33	66.67	66.67
SO_2	33.33	33.33	66.67	66.67

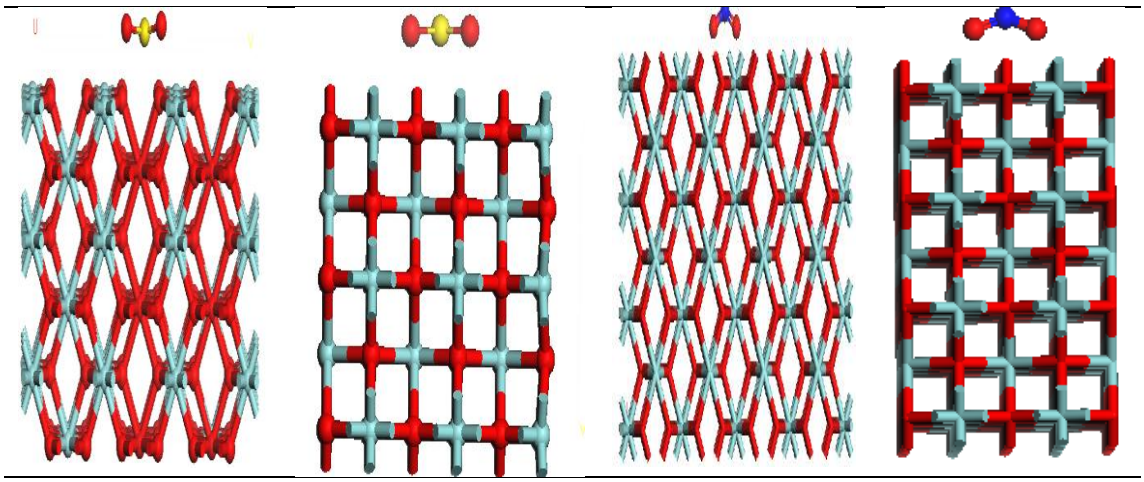

(a) **(b)** **(c)** **(d)**

Figure 3. Equilibrium adsorption configurations of molecules: (a) and (b) are for SO_2 (side and top view respectively), (c) and (d) for NO_2 (side and top view respectively)

Table 4. Calculated adsorption parameters for the interaction of the gas molecules with the ZrO_2 (1 1 0) surface

	Molecules	
Properties	SO_2	NO_2
Total potential energy (kcal/mol)	-87.57	-77.87
Energy of molecule (kcal/mol)	-21.34	-20.37
Energy of ZrO_2 (1 1 0) surface (kcal/mol)	0.00	0.00
Adsorption energy (kcal/mol)	-66.23	-57.50
Binding energy (kcal/mol)	66.23	57.50
Bond length between gas molecules and ZrO_2 (1 1 0) (Å)	3.51	3.55

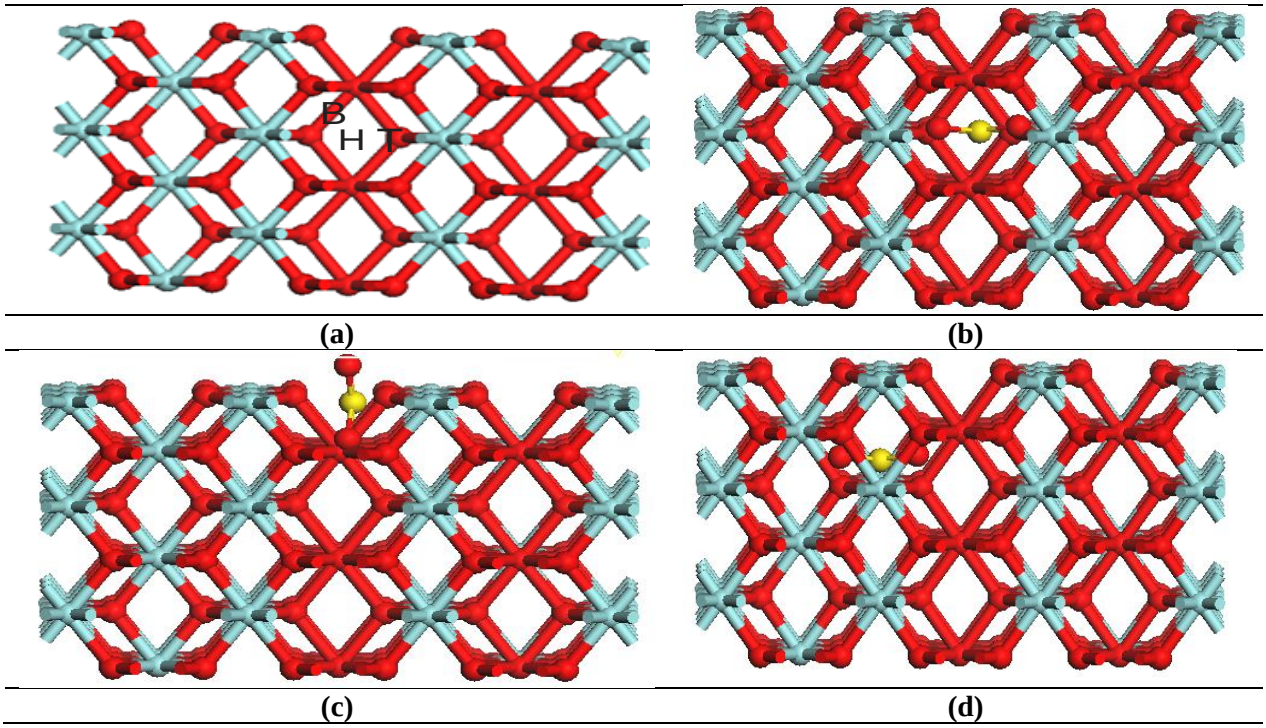

Figure 4. Relaxed structure of zirconia showing: (a) the three adsorption sites: hollow (H), bridge (B) and on top (T); (b) SO_2 parallel to ZrO_2 (1 1 0) with angle O-S-O facing downward; (c) SO_2 perpendicular to ZrO_2 (1 1 0); (d) SO_2 parallel to ZrO_2 (1 1 0) with angle O-S-O facing upward

Table 5. Bond lengths (Å) and bond angles (°) of optimized molecules before and after adsorption on ZrO_2 (1 1 0) surface

Geometric parameter	SO_2	NO_2	ZrO_2-SO_2	ZrO_2-NO_2
S-O	1.43	-	1.80	-
N-O	-	1.21	-	1.51
O-S-O	119.30	-	110.04	-
O-N-O	-	128.14	-	131.30

3. Computational Methods

3.1 Quantum chemical calculations

Density functional theory calculations using the double numerical polarization (DNP) basis set from Material Studio 7.0 (Accerys, Inc.) were conducted [36]. The molecules where only subjected to DFT calculations after they have been geometrically fine-tuned to achieve energetically low and stable structures [37]. Additionally, the PCM (Polarization continuum Model) was applied [38]. The energy of the highest occupied molecular orbital (E_H), energy of the lowest unoccupied molecular orbital (E_L), separation energy (ΔE), and parameters that provide information about molecular reactivity, such as electronegativity (χ), ionization potential (I), electron affinity (A), hardness (η), softness (σ), electrophilicity index (ω), and nucleophilicity (ε), were calculated using equations (1–7) in this study [39–41].

$$I = -E_H \quad (1)$$

$$A = -E_L \quad (2)$$

$$\chi = \frac{(I+A)}{2} = -\frac{E_L+E_H}{2} \quad (3)$$

$$\eta = \left(\frac{I-A}{2}\right) = -\frac{E_L-E_H}{2} \quad (4)$$

$$\sigma = \frac{1}{\eta} \quad (5)$$

$$\omega = \frac{\mu^2}{2\eta} = \frac{E_{HOMO}+E_{LUMO}}{8} = \frac{\chi^2}{2\eta} \quad (6)$$

$$\varepsilon = \frac{1}{\omega} \quad (7)$$

Global softness, which is the inverse of chemical hardness, can be used to quantify the degree of polarizability [42–43]. Global characteristics such as the energy of back donation ($\Delta E_{b\text{-}d}$) and the fraction of electrons transferred (ΔN_{max}) between each gas molecule and zirconia surface were calculated from global hardness and electronegativity values as shown in equations (8–9) [44]:

$$\Delta N_{max} = \frac{\chi}{2\eta} \quad (8)$$

$$\Delta E_{b-d} = -\frac{\eta}{4} = \frac{1}{8}(E_H - E_L) \quad (9)$$

The finding that an electron will tend to diffuse if it is introduced to an N- electron molecule in order to lower the energy of the resulting (N + σ)-electron system is the basis for the Fukui function. Given the accompanying changes in electron density, the finite difference approximation was used to determine the nucleophilic (f^+) and electrophilic (f^-) Fukui functions as follows [45–49]:

$$f^+ = \frac{(\delta p_r)}{(\delta N)v^+} = q(N+1)-q(N) \quad (10)$$

$$f^- = \frac{(\delta p_r)}{(\delta N)v^-} = q(N)-q(N-1) \quad (11)$$

where q(N+1), q(N), and q(N-1) stand for the atom's corresponding Mulliken, Hirshfield and electron density charges. The second order Fukui function was used to further define the electrophilic or nucleophilic nature of the entire molecule (global reactivity) as in equation (12):

$$\Delta f(r) = f^+ - f^- = f^2 \quad (12)$$

3.2 Molecular dynamic (MD) simulation

The Forcite module in Acceryls Material Studio 7.0 was used to carry out the MD simulation investigations of the interaction between the adsorbate gases and the zirconia surface with a goal to determining the lowest configuration adsorption energy [50]. Prior to the simulation investigations, the structures (adsorbate gases and zirconia surface) were improved geometrically using the COMPASS force field (condensed-phase optimized molecular potentials for atomistic simulation research) [30]. In order to replicate a representative portion of an interface free from any arbitrary border effects, ZrO_2 (1 1 0) was employed for the research in a simulation box (7 x 4Å) with periodic boundary conditions [22]. The NVT conical ensemble simulation at 350K with a time step of 1fs and a simulation length of 5ps were employed using the clever algorithm [51-54]. Every 250 steps, the system was quenched, and the adsorption energy (E_{ads}) of the molecules on ZrO_2 (1 1 0) was determined by averaging the five energies with the lowest values in accordance with equation 13 [24].

$$E_{ads} = E_{tot} - (E_{mol} + E_{sur}) \quad (13)$$

Where E_{sur} is the energy of the zirconia surface without the gas molecule and E_{mol} is the energy of the free gas molecule, E_{tot} is the total energy of the gas molecule adsorbed on the zirconia surface.

Equation 14 shows that binding energy is the opposite of adsorption energy.

$$E_{binding} = -E_{ads} \quad (14)$$

4. Conclusion

The adsorption mechanisms of SO_2 and NO_2 on zirconia surface have been predicted using density functional theory and molecular dynamic simulation methods. Through the process of physical adsorption, the investigated molecules were bound to the zirconia surface. The adsorption energies were determined via MD simulation and the determined DFT parameters agreed well in their trends. The molecules' adsorption strengths on the zirconia surface occur in the following order: $SO_2 > NO_2$.The fact that SO_2 is greater than NO_2 in E_{ads} is due to the fact that S is less electronegative than N and therefore more nucleophilic in nature. The geometrical study shows that the molecules strongly physisorb on the zirconia surface. It is suggested that the orientation of the molecules during interaction is that both molecules orient parallel to the surface (O-S-O and O-N-O angles facing upward), with S for SO_2 and N for NO_2 respectively binding to the surface. Since from this theoretical study, SO_2 and NO_2 can be sensed and adsorbed from the atmospheric environment, ZrO_2 (1 1 0) might be used for this purpose, according to both DFT and molecular dynamic simulation results.

Acknowledgements

Technical support by Dr. David E. Arthur, Department of Pure and Applied Chemistry, University of Maiduguri, Nigeria is gratefully acknowledged.

References

[1] A. Raval and V. Ramanathan, Observational determination of the greenhouse effect. *Nature* 342 (1989) 758-761. doi: 10.1038/342758a0.

[2] A. C. Stern, R. W. Bubel, D. B. Turner, D. L. Fox, Fundamentals of air pollution, 3rd ed., Academic press, New York (1997).

[3] Defra, RoTAP. Review of Transboundary Air Pollution: Acidification, Eutrophication, Ground Level Ozone and Heavy Metals in the UK. Contract Report to the Department for Environment, Food and Rural Affairs. Centre for Ecology and Hydrology (2012).

[4] G. P. Dohmen, M. C. Neill and S. Bell, J. N. B, Air Pollution Increases Aphis fabae pest potential. *Nature* 307 (1984) 52-53.

[5] A. K. Mishra and S. R. Prabhu, Study of CO_2 adsorption on low cost graphite nanoplatelets. *International Journal of Chemical Engineering and Application*, 1(3) (2010) 266-269. doi: 10.7763/IJCEA.2010.V1.46.

[6] C. W. Skarstrom, Press swing adsorption progress for air separation," U.S. Patent 2 944627 (1960).

[7] R. Sharma, T. Segado, M. P. Delplancke, H. Terryn, G. V. Baron and J. Cousin-Saint-Remi, Hydrogen chloride removal from hydrogen gas by adsorption on hydratedion-exchanged zeolites. *Chemical Engineering Journal* 381 (2020) 122512. doi: 10.1016/j.cej.2019.122512.

[8] Kh. M. Eid and H. Y. Ammar, Adsorption of SO_2 on Li atoms deposited on MgO (100) surface: DFT calculations. *Applied*

Surface Science 257 (2011) 6049-6058. doi: 10.1016/j.apsusc.2011.01.122.

[9] P. F. Manicone, P. R. Iommetti, L. Raffaelli, An overview of zirconia ceramics: Basic properties and clinic applications. *Journal of Dentistry* 35 (2007) 819-826. doi: 10.1016/j.jdent.2007.07.008.

[10] C. Piconi and G. Maccauro, Zirconia as a ceramic biomaterial. *Biomaterials* 20 (1999). 1-25.

[11] B. Bachilla-Baeza, I. Rodriguez-Ramos and A. Guerreo-Ruiz, Interaction of carbon dioxide with the surface of zirconia polymorphs *Langmuir* 14 (1998) 3556-3564. doi: 10.1021/la970856q.

[12] V. Bolis, G. Magnacca, G. Gerrato and C. Morterra, Microcalorimetric and IR-spectroscopic study of the room temperature adsorption of CO_2 on pure and sulphated t-ZrO_2. *Thermochimaca Acta* 379 (2001) 147-161. doi: 10.1016/S0040-6031(01)00613-X.

[13] K. Pokrovski, K. T. Jung and A. T. Bell, Investigation of CO and CO_2 adsorption on tetragonal and monoclinic zirconia. *Langmuir* 17(14 (2001) 4297-4303. doi: 10.1021/la001723z.

[14] F. G. R. Gimblett, A. A. Rahman and K. S W. Sing, The origin of porosity in hydrous zirconia gels. *Journal of Colloid and Interface Science* 8 (1981) 337-345.

[15] P. Banerjee, K. S. Sourav, G. Pritam, H. Abhiram and G. M. Naresh, Density functional theory and molecular dynamic simulation study on corrosion inhibition of mild steel by mercapto-quinoline Schiff base corrosion inhibitor. *Physica. E*, 66 (2015) 332-341. doi: 10.1016/j.physe.2014.10.035.

[16] U. Umaru, and A. M. Ayuba, Computational study of anticorrosive effects of some thiazole derivatives against the corrosion of aluminium. *RHAZES: Green and Applied Chemistry*, 10 (2020) 113-128. doi: 10.48419/IMIST.PRSM/rhazes-v10.23814.

[17] O. Dagdag, A. El Harfi, M. El Gouri, Z. Safi, R. T. Jalgham, N. Wazzan, C. Verma, E. E. Ebenso and U. P. Kumar, Anticorrosive properties of Hexa (3-methoxy propan-1, 2-diol) cyclotri-phosphazene compound for carbon steel in 3% NaCl medium: gravimetric, electrochemical, DFT and Monte Carlo simulation studies. *Heliyon* 5 (2019) e01340. doi: 10.1016/j.heliyon.2019.e01340.

[18] N. Khalil, Quantum chemical approach of corrosion inhibition. Electrochim. *Acta*, 48 (2003) 2635e2640. doi: 10.1016/s0013-4686(03)00307-4.

[19] F. E. Awe, S. O. Idris, M. Abdulwahab, E. E. Oguzie, Theoretical and experimental inhibitive properties of mild steel in HCl by ethanolic extract of Bosciasenegalensis, *Cogent Chemistry* 1 (2015) 1112676. doi: 10.1080/23312009.2015.1112676.

[20] A. M. Ayuba and M. Abubakar, Computational study for molecular properties of some of the isolated chemicals from leaves extract of Guiera Senegalensis as aluminium corrosion inhibitor. *Journal of Science and Technology* 13(1) (2021) 47-56. doi: 10.30880/jst.2021.13.01.006.

[21] T. A. Nyijime and A. M. Ayuba, Quantum chemical studies and molecular modeling of the effect of coriandrum sativum L. compounds as corrosion inhibitors on aluminum surface. *Applied Journal of Environmental Engineering Sciences* 6(4) (2020) 344-355.

[22] M. K. Awad, Quantum chemical studies and molecular modelling of the effect of polyethylene glycol as corrosion inhibitors of an aluminium surface. *Canadian Journal of Chemistry* 91 (2013) 283-291. doi: 10.1139/cjc.2012-0354.

[23] C. B. Verma, M. A. Quraishi and A. Singh, 2-Aminobenzene-1,3-dicarbonitriles as green corrosion inhibitor for mild steel in 1 M HCl: Electrochemical, thermodynamic, surface and quantum chemical investigation. *Journal of Taiwan Institute of Chemical Engineering* 4 (2015) 229-239. doi:10.1016/j.jtice.2014.11.029.

[24] U. Umaru and A. M. Ayuba, Modeling vitexin and isovitexin flavones as corrosion inhibitors for aluminium metal. *Karbala International Journal of Modern Science* 7(3) (2021) 206-215. doi: 10.33640/2405-609X.3119.

[25] B. Gómez, N. V. Likhanova, M.A. Domínguez-Aguilar, R. Martínez-Palou, A. Vela and J. L. Gazquez, Quantum chemical study of the inhibitive properties of 2-pyridyl-azoles. *Journal of Physical Chemistry B* 110 (2006) 8928-8934. doi: 10.1021/jp057143y.

[26] N. O. Obi-Egbedi, I. B. Obot, M. I. El-Khaiary, Quantum chemical investigation and statistical analysis of the relationship between corrosion inhibition efficiency and molecular structure of xanthene and its derivatives on mild steel in sulphuric acid. *Journal of Molecular Struct*ure 1002 (2011) 86-96. doi: 10.1016/j.molstruc.2011.07.003.

[27] J. Frau, D. Glossman-Mitnik, Conceptual DFT descriptors of amino acids with potential corrosion inhibition properties calculated with the latest minnesota density functionals. *Front. Chem*. 5 (2017) 16.

[28] L. Guo, Z. S. Safi, S. Kaya, W. Shi, B. Tüzün, N. Altunay, Anticorrosive effects of some thiophene derivatives against the corrosion of iron: a computational study. *Front. Chem*. 6 (2018) 155.

[29] T. Y. Mi, D. M. Triet, N. T. Tien, "Adsorption of gas molecules on penta-graphene nanoribbon and its implication for nanoscale gas sensor," *Physics Open*, vol. 2 pp. 100014, 2020, doi: 10.1016/j.physo.2020.100014.

[30] L. Guo, X. Ren, Y. Zhou, S. Xu, Y. Gong, S. Zhang, Theoretical evaluation of the corrosion inhibition performance of 1,3-thiazole and its amino derivatives. *Arabian Journal of Chem*istry 10 (2015) 121–130. doi: 10.1016/j.arabjc.2015.01.005

[31] M. E. Belghiti, Y. El Oudadi, S. Echihi, A. Elmelouky, H. Outada, Y. Karzazi, M. Bakasse, C. Jama, F. Bentiss, A. Dafali, Anticorrosive properties of two 3,5- dissubstitud-4-amino-1,2,4-triazole derivatives on copper in hydrochloric acid environment: Ac impedance, thermodynamic and computational investigations. *Surface Interface* 21 (2020) 100692. doi: 10.1016/j.surfin.2020.100692.

[32] P. Pyykko, M. Astumi, Molecular single bond covalent radii for elements 118. *Chemistry*, 15(1) (2009) 186-197. doi: 10.1002/chem.200800987.

[33] H. Ye, L. Liu, Y. Xu, L. Wang, X. Chen, K. Zhang, Y. Liu, S. W. Koh, G. Zhang, SnSe monolayer: A promising candidate of SO_2 sensor with high adsorption quantity. *Applied Surface* 484 (2019) 33-38. doi: 10.1016/j.apsusc.2019.03.346.

[34] A. Kuang, M. Kuang, H. Yuan, G. Wang, H. Chen and X. Yan, Acidic gases (CO_2, NO_2 and SO_2) capture and dissociation on metal decorated phosphorene. *Applied Surface Science* 2017. doi: 10.1016/j.apsusc.2017.03.135.

[35] V. V. Kulishi, O. I. Malyi, C. Persson, P. Wu, Adsorption of metal adatoms on single-layer phosphorene. *Physical*

Chemistry Chemical Physics 17 (2015) 992-1000. doi: 10.1013/C4CP038890H.

[36] Q. Zhao, T. Tang, P. Dang, Z. Zhang, F. Wang, The corrosion inhibition effect of triazinedithiol inhibitors for aluminium alloy in a 1MHCl solution. *Metals* 7(2) (2017) 42. doi: 10.3390/met7020044.

[37] H. B. Schlegel, Optimization of equilibrium geometries and transition structures. *Journal of Computational Chemistry* 3(2) (1982) 214-218. doi: 10.1002/jcc.540030212.

[38] E. Canses, B. Mennucci and J. Tomasi, A new integral equation formalism for the polarizable continuum model: Theoretical background and applications to isotropic and anisotropic dielectrics. *Journal of Chemical Physics* 107 (1997) 3032-3041. doi: 10.1063/1.474659.

[39] N. P. Bellafont, F. Illas, P. S. Bagus, Validation of Koopmans' theorem for density functional theory binding energies. *Physical Chemistry Chemical Physics* 17 (2015) 4015e-4019. doi: 10.1039/C4CP05434B.

[40] L. H. Madkour, I. H. Elshamy, Experimental and computational studies on the inhibition performances of benzimidazole and its derivatives for the corrosion of copper in nitric acid. *International Journal of Industrial Chemistry*, 7 (2016) 195e221. doi: 10.1007/s40090-015-0070-8.

[41] A. A. Khadom, Quantum chemical calculations of someamines corrosion inhibitors/copper Alloy interaction in hydrochloric acid. *Journal of Material and Environmental Science* 8 (2017) 1153e1160. http://www.jmaterenvironsci.com.

[42] A. M. Ayuba, A. Uzairu, H. Abba and G. A. Shallangwa, Hydroxycarboxylic acids as corrosion inhibitors on aluminium metal: a computational study. *Journal of Material and Environmental Science* 9 (2018) 3026e3034. http://www.j,materenvironsci.com.

[43] H. Lgaz, R. Salghi, A. Chaouiki, S. Shubhalaxmi, K. S. Jodeh, Bhat, Pyrazoline derivatives as possible corrosion inhibitors for mild steel in acidic media: a combined experimental and theoretical approach. *Cogent Engineering*, 5 (2018) 1441585. doi: 10.1080/23311916.2018.1441585.

[44] L. Guo, Z. S. Safi, S. Kaya, W. Shi, B. Tuzun, N. Altunay, C. Kaya, Anticorrosive effects of some thiophene derivatives against the corrosion of iron: a computational study. Frontier Chemistry 6 (2018) 155. doi: 10.3389/fchem.2018.00155.

[45] K. F. Khaled, Studies of iron corrosion inhibition using chemical, electrochemical and computer simulation techniques. *Electrochim. Acta* 22 (2010) 6523.

[46] R. G. Pearson, Hard and soft acids and bases *J. Am. Chem. Soc*., 85(22) (1963) 3533-3539.

[47] R. G. Parr, L. Szentpaly, S. Liu, Electrophilicity index. *J. Am. Chem. Soc*, 121 (1999) 1922-1924.

[48] G. Bereket, E. Hur, C. Ogretir, Quantum chemical studies on some imidazole derivatives as corrosion inhibitors for iron in acidic medium, *J. Mol. Struct. (Theochem).* 578 (2002) 79e88. https://doi.org/10.1016/S0166-1280(01)00684-4.

[49] M. Belghiti, S. Echihi, A. Dafali, Y. Karzazi, M. Bakasse, H. Elalaoui-Elabdallaoui, Computational simulation and statistical analysis on the relationship between corrosion inhibition efficiency and molecular structure of some hydrazine derivatives in phosphoric acid on mild steel surface. *Applied surface science* 491 (2019) 707-22.

[50] L. O. Olasunkanmi, I. B. Obot, M. M. Kabanda and E. E. Ebenso, Some quinoxalin-6-yl derivatives as corrosion inhibitors for mild steel in hydrochloric acid: experimental and theoretical studies. *Journal of Physical Chemistry C* 119 (2015) 16004-16019. doi: 10.11021/acs.jpcc.5b03285.

[51] G. Bereket, C. Ogretir and A. Yurt, Quantum mechanical calculations on some 4-methyl-5-substituted imidazole derivatives as acidic corrosion inhibitor for zinc. *Journal of Molecular Structure (Theochem)* 571 (2001) 139-145. doi: 10.1016/s01661280(01)005528.

[52] S. A. Siadati, A. Mirabi, Diels-Alder versus 1, 3-dipolar cycloaddition pathways in the reaction of C20 fullerene and 2-furan nitrile oxide. *Progress in Reaction Kinetics and Mechanism*, 40(4) (2015) 383-390. http://dx doi:10.3184/146867815X14413752286065.

[53] P. Pakravan, S. A. Siadati, The possibility of using C20 fullerene and graphene as semiconductor segments for detection, and destruction of cyanogen-chloride chemical agent. *Journal of Molecular Graphics and Modelling*, *75*, (2016)80-84. http://dx.doi.org/doi:10.1016/j.jmgm.2016.12.001.

[54] E. Vessally, S. A. Siadati, A. Hosseinian, L. Edjlali, Selective sensing of ozone and the chemically active gaseous species of the troposphere by using the C20 fullerene and graphene segment. *Talanta*, 162 (2016) 505-510. http://dx.doi.org/10.1016/j.talanta.2016.10.010.